Electrical conductivity in patterned silver–mesoporous titania nanocomposite thin films: towards robust 3D nano-electrodes†

Eduardo D. Martínez,[a] Leticia Granja,[b] Martín G. Bellino[a] and Galo J. A. A. Soler-Illia*[a]

Received 8th June 2010, Accepted 3rd September 2010
DOI: 10.1039/c0cp00824a

The space-resolved electrical conductivity of patterned silver nanoparticle (NP) arrays embedded in mesoporous TiO_2 thin films was locally evaluated using a conductive-tip AFM. A remarkable conductivity dependence on the film mesostructure and metal NP loading was observed, confirming a three-dimensional current flow throughout the nanocomposite.

Introduction

The unique electronic, optical, catalytic and chemical properties of metallic nanoparticles (NP) embedded in oxide thin films represent a great promise for advanced applications such as nanoelectronics, bioanalysis or optoelectronics. For the development of NP-based electronics, it is desirable to engineer three-dimensional arrays of metal nanoparticles that can be used as highly controlled wires, circuits and/or electrodes. Several strategies for supporting metal nanoparticles into 3D arrays have been developed during recent years including the use of self-assembled polyelectrolytes,[1] polymer matrices[2] and inorganic mesoporous frameworks to impart an ordered distribution.[3–10] Embedding NP within thin films permits to exploit their properties derived from size or confinement and protect them from the environment. Mesoporous thin films (MTF) provide restricted chemical environments and grant accessibility to ions or molecules due to their controlled pore size domains, constituting ideal matrices for metallic NP inclusion.

The primary requirement for optimum electrical performance is a closely packed NP assembly. In addition, the arbitrary patterning of NP arrays is of paramount importance for electronic or analytical applications that require a precise spatial location of nanospecies such as microarrays, nanoelectronic circuits, SERS devices, lab-on-chip, *etc*. In this work, we explore the 3D electronic conductive properties of patterned nanocomposites formed by TiO_2 MTF loaded with Ag NP by the Photocatalysis-Assisted Mesopore Patterned Array (PAMPA) lithography procedure previously developed.[11] We performed scanning probe microscopy measurements to study for the first time the localized electrical properties of the NP–MTF patterned nanocomposite, and their dependence with film structure and Ag loading.

Experimental section

Titania MTF were produced by dip-coating, as reported in previous work (see detailed preparation in ESI†).[12–16] Film thickness was varied by modifying the dip-coating speed. Porosity was controlled by tuning the molar ratio between the template and the inorganic precursor (s = [template]/[Ti]). MTF were characterized by SAXS, X-Ray Reflectometry (XRR), SEM, TEM and ellipsoporosimetry analysis (EPA) to determine mesostructure, thickness, pore volume and pore size distribution.[17]

Two types of nanocomposite film samples were produced in this study. The first one consisted of an MTF directly deposited on conductive silicon (N-doped P (100) 3–7 Ω cm, University Wafer, South Boston, MA), in order to analyze the conductivity behaviour in the direction normal to the substrate. The second set of samples was designed to study the lateral conductivity along the film plane. In this case, a 50 nm thick intermediate layer of non-mesoporous SiO_2 was first deposited in order to isolate electrically the TiO_2 MTF from the silicon substrate (Fig. 1A and B).

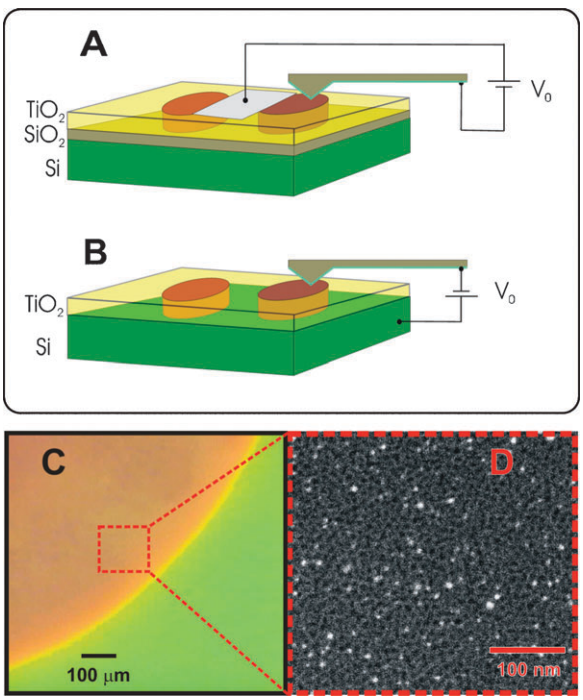

Fig. 1 Upper frame: scheme of the electric configuration used to perform the CAFM measurements for (A) lateral and (B) vertical current scanning. The circles represent the Ag NP loaded regions of the film with different infiltration times. Lower frame: (C) optical image of the TiO_2 MPF after 90 min of UV exposure, presenting a patterned circle of Ag NP–titania composite, (D) FE-SEM top-view of the patterned region of the sample shown in C. No formation of silver paths on the surface is observed. Note that some pores are tipped by isolated nanoparticles (bright spots) occupying the upper pore layer.

[a] *Gerencia de Química, CNEA, CAC, Av., Gral Paz 1499, San Martín B1650KNA, Argentina. E-mail: gsoler@cnea.gov.ar*
[b] *Departamento de Materia Condensada, Gerencia de Investigación y Aplicaciones, CNEA, CAC, Buenos Aires, Argentina*
† Electronic supplementary information (ESI) available: Detailed film preparation and characterization, including pore filling assessment. See DOI: 10.1039/c0cp00824a

The PAMPA method consists in an Ag^+ impregnation step, followed by UV illumination through a lithography mask.[11] TiO_2 MTF were first immersed in 1 M $AgNO_3$ ethanol : water 1 : 1 solution for at least 10 min. Films were subsequently placed in a plastic container and a printed polyacetate mask was positioned over the film; mask adhesion was assured by capillary forces. The ensemble was covered with the Ag^+ solution and located 2 cm beneath the UV lamp (Philips 15 W, λ_{max} = 355 nm). UV-excited electrons in the anatase TiO_2 assist Ag^+ photoreduction in the presence of ethanol.[18–21] The use of the mask provides the means to produce an arbitrarily patterned metallic silver array within the MTF.[11] Two circular patterns with different Ag NP loading were produced in each film (Fig. 1C). After removing the mask, samples were rinsed with ethanol and cleaned with optical tissue cleaning paper to remove any excess of particles formed on the surface (Fig. S2, ESI†).[6] Finally, samples were washed by placing them in a 1 : 1 ethanol : water mixture for one hour under stirring. Energy Dispersive Spectroscopy (EDS) measurements were performed on each sample to establish the Ag : Ti ratio after infiltration (metallic Ag^0, adsorbed Ag^+ ions and Ag_2O also present in the system). The pore volume before and after NP loading was determined by XRR measurements of the critical angle in bare and Ag-loaded films (see ESI†), as previously reported.[6]

Conducting-tip atomic force microscopy (CAFM) images were acquired with a Solver Pro NT-MDT scanning probe microscope. Electric current (I) and topography were simultaneously scanned with a Pt coated Si tip in contact mode under a dry air flow environment. Scannings were performed applying a constant voltage (V_0) between the nanoscale tip (curvature radius *ca.* 35 nm) and an electrical contact located remotely in the sample. This technique made also possible to evaluate the current–voltage (I–V) curves at different xy tip positions on the sample surface. For the lateral conductivity measurements, a silver electrode was sputtered on an edge of the surface of the silver-infiltrated circles. In the case of the vertical conductivity measurements, the silicon substrate was contacted with silver paint to a conductive sample holder at V_0 with respect to the tip. Both configurations are schematised in Fig. 1.

Results and discussion

A set of titania mesoporous films with different thickness and porous volume in the range of 20–30% was prepared by dip-coating in the presence of block copolymer F127 as the templating agent, followed by thermal treatment to 350 °C (Table 1). Films were then subjected to the PAMPA method (Ag^+ adsorption followed by UV patterning) for 15 and 90 minutes.

CAFM measurements of the samples were performed to evaluate the electrical conductivity inside, outside and especially at the border of the photolithographically infiltrated silver patterns. No topographical difference was appreciated by FE-SEM between the infiltrated and non-infiltrated regions on the samples. However the simultaneous current scanning displayed a clear conduction contrast at the edge of the patterning in some samples, depending on the silver loading. The scanning current profiles along these edges for samples with different Ag loading are summarised in Fig. 2. The bias voltage applied, V_0 = 10 V, is the highest allowed in this CAFM equipment.

The study performed for the lateral conductivity, samples A_L to D_L in Fig. 2, showed that the average value and the homogeneity of the current density increase with irradiation time, film thickness, and accessibility of the porous structure (*i.e.*, pore volume and interpore neck size). In addition, the observed dependence with film thickness suggests that conduction is developing three-dimensionally through interconnected Ag particles within the nanocomposite film volume. In the case of thinner films, it was not possible to define the border for the thinner films, even when conductivity in the central region of the circle was observed. On the other hand, EDS results confirm that Ag loading increases remarkably with the irradiation time but it seems not to be critically affected by pore interconnectivity. However, the absolute value and the homogeneity of the scanning current increases with both the irradiation time and pore accessibility. In all cases, the variations on the probe–electrode distance were not appreciated on the scanning current due to the tip–sample contact resistance and Ag loading effects.

The topographical and electrical characteristics are compared in Fig. 3a and b for a circular patch subjected to 90 minutes of Ag^+ photoreduction (sample B_L). The NP filling fraction of the pore volume of this sample determined by XRR is, 55 ± 2%, in excellent agreement with the pore filling estimated from EDS results (see ESI†). Even in the case of the highest conduction performance obtained, no topographical evidences of the silver circle appear, in agreement with the FE-SEM images. It is worth noting that no continuous nanoparticle path is detectable on the film surface.

Current–voltage curves in the ±10 V range were performed in silver loaded and unloaded regions for all the samples. In all cases, no current was measured for the unloaded regions. Inside the silver-loaded regions, the I–V curves were strongly dependent of the homogeneity of the conductivity. Thus the most reproducible and consistent I–V curves inside the conductive regions were obtained in sample B_L (Fig. 3c). Note that this is a two points measurement, where the nanoscale tip–sample contact is a highly resistive junction involving

Table 1 Structural data of the mesoporous thin films obtained from EPA measurements.[17] Subscripts L and V identify the samples with lateral and vertical electrical configuration respectively

	s	V_{dip}/mm s^{-1}	Thickness/nm	V_{pore} (%)	D_{pore}/nm	D_{neck}/nm
A_L	0.0075	0.6	102	28	9.2	5.8
B_L	0.0075	2	179	35	8.8	6.2
C_L	0.005	2	166	18	8.4	5.6
D_L	0.005	0.6	77	19	9.8	5.6
E_V	0.0075	2	185	32	9.8	5.8

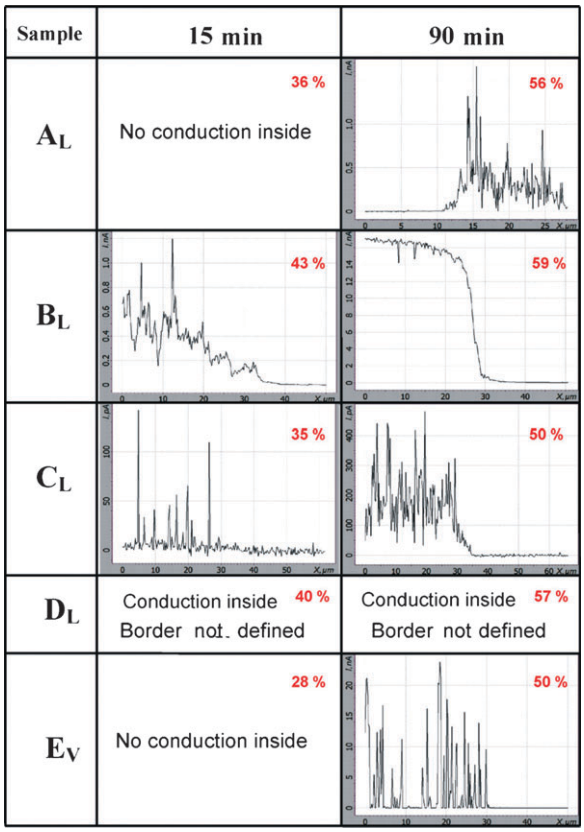

Fig. 2 Summarised results of the lateral (A_L to D_L) and vertical (E_V) conductivity for the samples studied comparing the scanning current profiles along the border of the patterned areas obtained by CAFM with V_0 = 10 V. The cases where the conduction border was not defined or no conduction was present at all in the Ag circle are also specified. Ag : Ti atomic fractions measured by EDS (relative uncertainty: 5%) are shown in red for each sample, in the upper right corner of each graph.

several different materials. The non-linear and asymmetric shape of this curve should be therefore mainly attributed to the contact resistance.

Vertical electrical transport studies (*i.e.*, across the film) were carried out in sample E_V, obtained in conditions similar to sample B_L, which had the highest lateral conduction performance. A lower NP loading is observed in the E_V sample with respect to B_L after 90 minutes irradiation due to differences in the substrate that affect the photoreduction process. The average value of the current in sample E_V is comparable to the Ag-laden region of sample B_L. However, in the E_V case, high current values are only observed in isolated conductive spots evenly distributed along the film surface. A comparison between the topography and current scanning across a border of the circle of the E_V sample after 90 minutes irradiation (Fig. S3b, ESI†) shows that the highly conductive spots do not correspond to agglomerated particles or any other surface feature. A similar "spotted" conductivity pattern is observed in the lateral conductivity experiments performed on the C_L sample (Fig. S3d, ESI†), which presents silver contents similar to those found in E_V (Fig. 2). This result suggests that in this range of NP loadings (Ag : Ti = 50%), percolation is possible but only few conductive paths are developed.

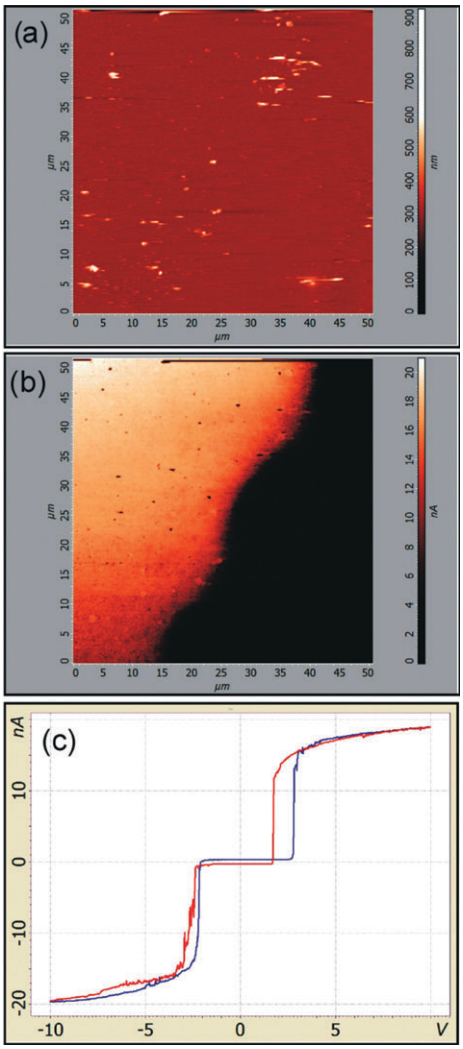

Fig. 3 CAFM images for lateral conduction of sample B_L after 90 minutes of photoreduction time. (a) Contact mode topography scanning and (b) current scanning at V_0 = 10 V. (c) Typical current–voltage curve measured within the conductive region.

Above this threshold loading, NP can grow along time, and eventually contact each other. GI-XRD experiments performed on B_L samples subjected to reduction for 15 and 90 minutes (Fig. S5, ESI†) show a narrowing of the (111) silver peak along reduction, demonstrating NP growth (from 5.0 ± 0.2 nm to 8.4 ± 0.6 nm, according to the Scherrer equation).

The vertical and lateral CAFM measurements presented here confirm that the current is developing through the film along the three dimensions. The study of the electrical transport properties of discontinuous metal films, metallic nanoparticle assemblies and composites of metallic and insulating nanoparticles have been treated both experimentally and theoretically.[22–27] The electrical transport properties depend on the metal filling fraction. A percolation threshold arises, below which the electrical resistance of the system can be seen as the series resistance of the insulating and metallic materials involved. In this case, the electrical transport behaviour is dominated by the nature of the insulating substrate or matrix. Above the percolation threshold, percolating conductive paths are created and the electrical resistance is

basically the parallel resistance of the insulating and conductive materials between the electrodes. The electrical properties in this case are akin to those of the bulk metal. The transition between the two transport regimes is not abrupt, being softened by electron transport processes that occur when isolated particles are close enough to percolate electrically. In particular, in the systems studied in this work, the interface effects play a fundamental role, and the electron transfer at the oxide–metal interface should be considered as an additional contribution to the transport behaviour. Thus, non-ohmic mechanisms can appear even in the percolating regime. Several processes have been proposed including variable range hopping conductivity, thermionic emission, tunnelling transport and thermally activated tunneling.[23–25] The temperature and electrical field dependence of the non-ohmic behaviour is the proper pathway to establish the mechanism involved.[25,26] Detailed electrical transport studies of these nanocomposite systems in order to determine the dominating electric transport processes are in progress. However, the high conductivity observed after 90 minutes irradiation for the majority of the samples, especially for sample B_L, and the presence of spotted patterns for the E_V and C_L samples suggest that the percolation threshold is obtained before a pore filling of 50%. Detailed experiments in order to precisely determine this threshold, and to correlate it with Ag NP pore volume filling are underway.

Conclusion

The localized conductivity of robust silver nanoparticle arrays embedded within titania mesoporous films has been explored using scanning probe microscopy techniques. An abrupt conductivity frontier is obtained between loaded and unloaded silver regions. The electrical conduction in the silver-oxide nanocomposites is not due to surface effects, as demonstrated by the absence of NP patterns on the film surface. Film architecture at the nanoscale clearly influences silver NP loading and thus the conductivity of the nanocomposite. From the dependence with the different structural parameters, it can be concluded that the electrical transport is developed in the three dimensions of the NP array, and that it improves with increasing silver loading, the section of the current flow and the accessible porous volume.

We have to remark that the size and resolution of the patterning is limited by the lithography technique used, so the highest potential of the method has not been reached yet. Further investigations need to be performed in order to understand the mechanisms involved in the charge transport phenomena. However, these results are promising for the design of nanostructured 3D electrodes with tailored conductivity for applications in electro-catalysis, MEMs, lab-on-chip, sensors, memories, nanocircuits, solar cells and devices needing precise spatial resolved conductivity.[28] In addition, the wide possibilities of tailoring MTF in features such as inorganic framework, mesopore size or surface nature permit to design the guest NP size, connectivity and NP–matrix interactions. These highly controlled new features can be exploited to tune the electrical or optical behaviour by a combination of size, confinement or NP–surface interaction effects.

Acknowledgements

Work funded by ANPCyT (PICT Nos 34518 and 00335, PAE 2006-37063-00038). E. D. M. acknowledges a doctoral fellowship from CONICET/ANPCyT. Authors thank ABTLuS (Campinas, Brazil), for funding XRR and SAXS measurements at the LNLS synchrotron, and M. Rosenbusch for help in contact deposition. L. G., M. G. B. and G. J. A. A. S-I. are members of CONICET.

References

1 T. C. Wang, M. F. Rubner and R. E. Cohen, *Langmuir*, 2002, **18**, 3370.
2 W. Caseri, *Macromol. Rapid Commun.*, 2000, **21**, 705.
3 Y. Plyuto, J. M. Berquier, C. Jacquiod and C. Ricolleau, *Chem. Commun.*, 1999, 1653.
4 J. Zhu, Z. Kónya, V. F. Puntes, I. Kiricsi, C. X. Miao, J. W. Ager, A. P. Alivisatos and G. A. Somorjai, *Langmuir*, 2003, **19**, 4396.
5 M. D. Pérez, E. Otal, S. A. Bilmes, G. J. A. A. Soler-Illia, E. L. Crepaldi, D. Grosso and C. Sanchez, *Langmuir*, 2004, **20**, 6879.
6 M. C. Fuertes, M. Marchena, M. C. Marchi, A. Wolosiuk and G. J. A. A. Soler-Illia, *Small*, 2009, **5**, 272.
7 M. Andersson, H. Birkedal, N. R. Franklin, T. Ostomel, S. Boettcher, A. E. C. Palmqvist and G. D. Stucky, *Chem. Mater.*, 2005, **17**, 1409.
8 A. L. Pénard, T. Gacoin and J. P. Boilot, *Acc. Chem. Res.*, 2007, **40**, 895.
9 H. Fan, K. Yang, D. M. Boye, T. Sigmon, K. J. Malloy, H. Xu, G. P. Lopez and C. J. Brinker, *Science*, 2004, **304**, 567.
10 Y. Kumai, H. Tsukada, Y. Akimoto, N. Sugimoto, Y. Seno, A. Fukuoka, M. Ichikawa and S. Inagaki, *Adv. Mater.*, 2006, **18**, 760.
11 E. D. Martínez, M. G. Bellino and G. J. A. A. Soler-Illia, *ACS Appl. Mater. Interfaces*, 2009, **1**, 746.
12 E. L. Crepaldi, G. J. A. A. Soler-Illia, D. Grosso, F. Ribot, F. Cagnol and C. Sanchez, *J. Am. Chem. Soc.*, 2003, **125**, 9770.
13 E. L. Crepaldi, G. J. A. A. Soler-Illia, D. Grosso and C. Sanchez, *New J. Chem.*, 2003, **27**, 9.
14 P. C. Angelomé, M. C. Fuertes and G. J. A. A. Soler-Illia, *Adv. Mater.*, 2006, **18**, 397.
15 F. Cagnol, D. Grosso, G. J. A. A. Soler-Illia, E. L. Crepaldi, F. Babonneau, H. Amenitsch and C. Sanchez, *J. Mater. Chem.*, 2003, **13**, 61.
16 M. C. Fuertes, F. J. López-Alcaraz, M. C. Marchi, H. E. Troiani, V. Luca, H. Míguez and G. J. A. A. Soler-Illia, *Adv. Funct. Mater.*, 2007, **17**, 1247.
17 C. Boissière, D. Grosso, S. Lepoutre, L. Nicole, A. B. Bruneau and C. Sanchez, *Langmuir*, 2005, **21**, 12362.
18 K. Matsubara, K. L. Kelly, N. Sakaia and T. Tatsuma, *Phys. Chem. Chem. Phys.*, 2008, **10**, 2263.
19 E. Stathatos, P. Lianos, P. Falaras and A. Siokou, *Langmuir*, 2000, **16**, 2398.
20 S. C. Chan and M. A. Barteau, *Langmuir*, 2005, **21**, 5588.
21 X. Chen and S. Mao, *Chem. Rev.*, 2007, **107**, 2891.
22 C. A. Neugebauer and M. B. Webb, *J. Appl. Phys.*, 1962, **33**, 74.
23 A. Zabet-Khosousi and A. A. Dhirani, *Chem. Rev.*, 2008, **108**, 4072.
24 K. Seal, M. A. Nelson, Z. C. Ying, D. A. Genov, A. K. Sarychev and V. M. Shalaev, *Phys. Rev. B: Condens. Matter*, 2003, **67**, 353181.
25 P. Bieganski, E. Dobierzewska-Mozrzymas, E. Pieciul and G. Szymczak, *Vacuum*, 2004, **74**, 211.
26 D. Greshnykh, A. Frömsdorf, H. Weller and C. Klinke, *Nano Lett.*, 2009, **9**, 473.
27 H. Wei and H. Eilers, *J. Phys. Chem. Solids*, 2009, **70**, 459.
28 P. Innocenzi, T. Kidchob, P. Falcaro and M. Takahashi, *Chem. Mater.*, 2008, **20**, 607.

